

Inverse Transfer Method Using Polymers with Various Functional Groups for Controllable Graphene Doping

Seong Kyu Lee¹, Jae Won Yang², Hyun Ho Kim¹, Sae Byeok Jo¹, Boseok Kang¹, Hyojin Bong¹, Hyo Chan Lee¹, Geunsik Lee², Kwang S. Kim^{3}, Kilwon Cho^{1*}*

- 1) Department of Chemical Engineering, Pohang University of Science and Technology (POSTECH),
Pohang, 790-784, Korea
- 2) Department of Chemistry, Pohang University of Science and Technology (POSTECH),
Pohang, 790-784, Korea
- 3) Department of Chemistry, Ulsan National Institute of Science and Technology (UNIST),
Ulsan, 689-798, Korea

A. Tuning the electrical properties of monolayer graphene using different functionalized polymers and stability

Graphene was synthesized on copper foil using the CVD process. PMMA was spin-coated onto one side of the graphene to form a supporting layer and was floated in a 0.1 M ammonium persulfate ((NH₄)₂S₂O₈) solution. After the copper foil had been etched away, the PMMA/graphene film was transferred to DI water for rinsing. Finally, the graphene film prepared with PMMA was transferred to a silicon wafer treated with hexamethyldisiloxane (HMDS), and the PMMA was removed by washing in acetone. Au electrodes with a defined channel length ($L = 30 \mu\text{m}$) and width ($W = 300 \mu\text{m}$) were patterned onto the transferred graphene film. Polymer solutions were deposited by spin-coating (at 1000rpm) onto the graphene channel and annealed for 10 min at 120°C.

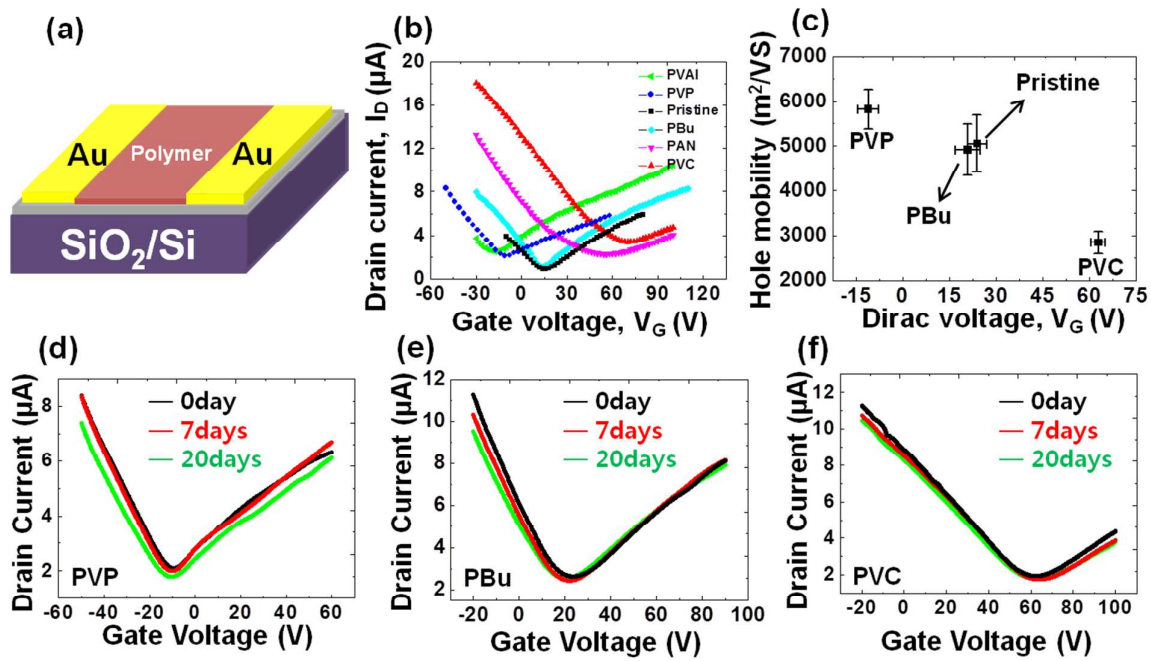


Figure S1. (a) Schematic diagram of the graphene FETs prepared with a polymer doping layer on the graphene channel. (b) Dirac voltage point shifts for monolayer graphene samples prepared with polymers having different functional groups. (PVAI = poly vinyl alcohol and PAN = polyacrylonitrile.) (c) Hole mobility and Dirac voltage point of pristine graphene and doped graphene by PVP, PBu or PVC. The transfer curve of graphene transistor doped by (d) PVP, (e) PBu or (f) PVC as a function of time at atmospheric pressure and room temperature. (black : 0 day, red : 7 days, green : 20 days)

B. Large-area graphene transfer *via* inverse transfer method (ITM)

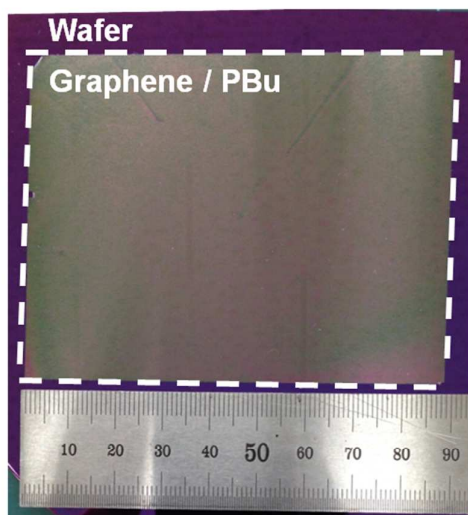


Figure S2. Large scale of (90mm X 60mm) transferred graphene with PBU using ITM on wafer.

The graphene is on the top of the surface and the PBU is between graphene and wafer.

C. The thickness of graphene/polymers

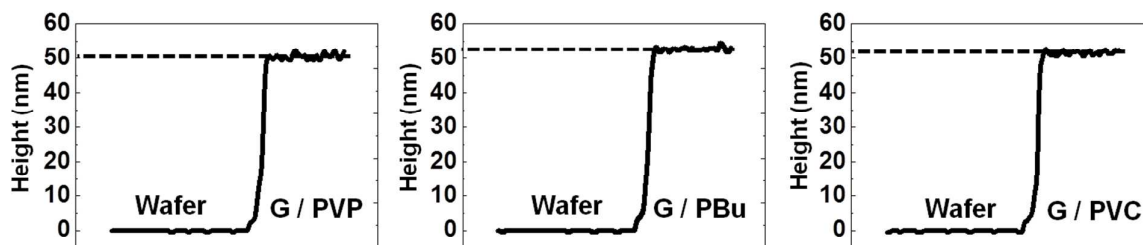
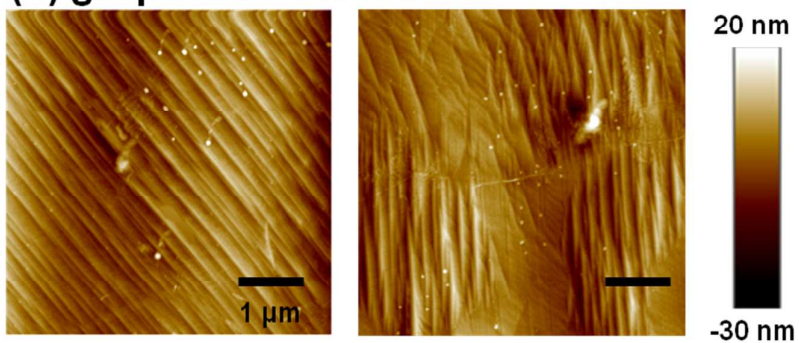


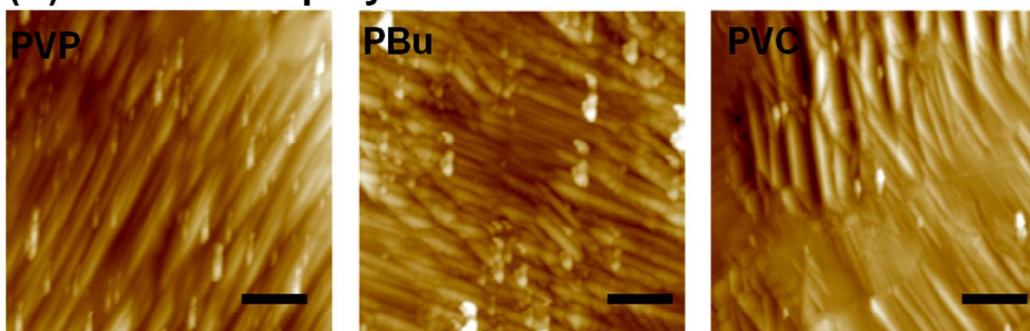
Figure S3. The Thickness of (a) graphene/PVP, (b) graphene/PBu and (c) graphene/PVC transferred by ITM.

D. Surface morphology analysis

(a) graphene / Cu foil



(b) transferred polymer on Si wafer



(c) transferred graphene / polymer on Si wafer

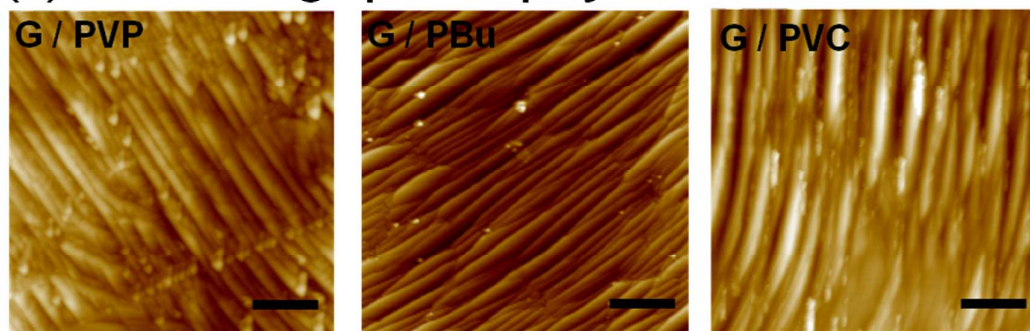


Figure S4. AFM images of (a) graphene on Cu foil after CVD growth, (b) inversely transferred polymers from Cu foil onto Si wafer substrate and (c) graphene/polymers transferred by ITM on Si wafer. The surface morphologies of polymers and graphene/polymers followed graphene/Cu foil surface morphology after transfer onto Si wafer.

E. Clean surface of graphene transferred by ITM

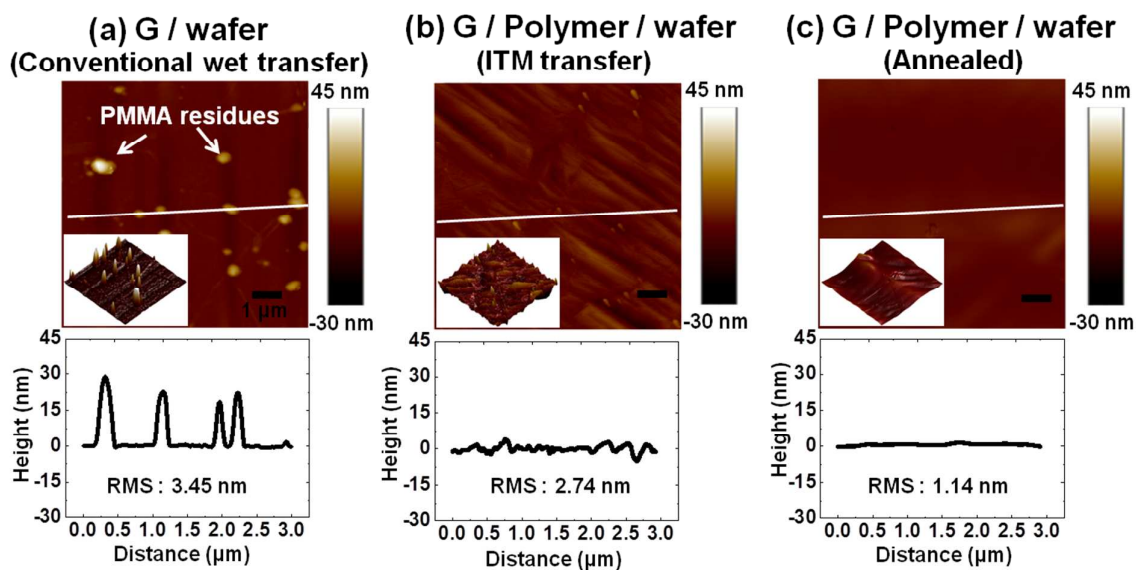


Figure S5. Surface of graphene transferred onto wafer by (a) conventional wet transfer method, (b) ITM and (c) annealed after ITM. From the conventional wet transfer method, PMMA residues (white arrows, 20~30 nm height) remained on the graphene surface. From the ITM, however, the graphene surface is clean without polymer residues. The graphene surface is flat and smooth after annealing.

F. Properties of graphene on polymer layer

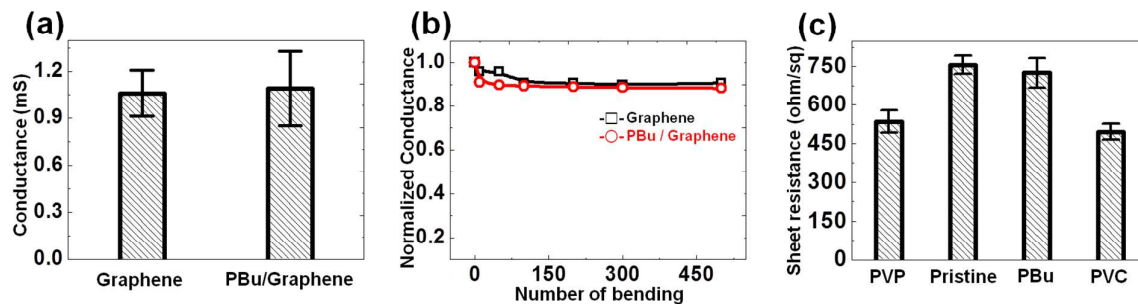


Figure S6. (a) Conductance of pristine graphene and PBu/Graphene on PET. (b) Bending test with a bending radius of 5mm to measure the change of conductance of pristine graphene (black) and PBu/Graphene (red) by number of bending. (c) The sheet resistance of pristine graphene, transferred and doped graphene by PVP, PBu or PVC.

G. Raman spectroscopy analysis for doping of graphene

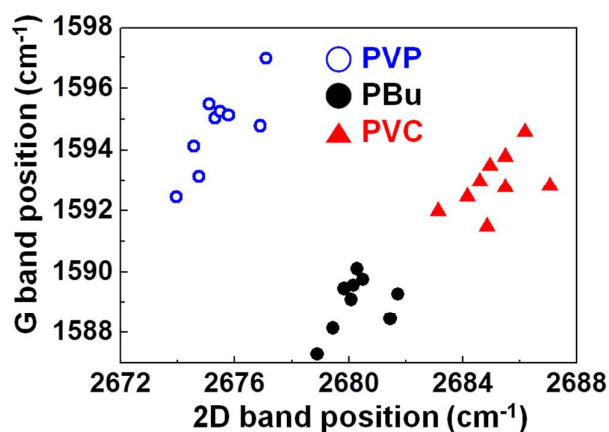


Figure S7. G and 2D band positions in the graphene transferred using the ITM with different polymers.

H. Theoretical calculation methods

All theoretical calculations were performed using the Vienna *ab initio* simulation package using pseudopotentials and a plane wave basis set.¹ Because the polymer was weakly physisorbed to the graphene, the van der Waals density functional theory was used to include London dispersion interactions between the polymer and graphene.² The optB86b-vdW functional was used for the exchange–correlation energy, and the projector augmented wave^{3,4} was used to model the electron–ion interactions. A cutoff energy of 400 eV was set for the plane wave basis. The total energies of the interface and reference systems were calculated using the equivalent lateral unit cell size and Brillouin zone sampling using a 3x3x1 k-point grid. A dipole correction was applied to avoid spurious interactions between the dipoles of repeated slabs along the direction normal to the graphene surface.

The polymer–graphene interface was modeled using 4×4, 6×6, or 8×8 graphene supercells with polymer layers that were separated from the neighboring polymers by more than 5 Å. We fully relaxed both the graphene and polymer layers until the forces were less than 0.01 eV/Å. All systems were modeled as crystallized polymers on graphene surface. The crystalline polymer structure was not expected to affect the model of the dipole moment introduced by the polymers because graphene doping is thought to be independent of the specific interface structure.

The calculated equilibrium bonding distances and binding energies revealed that the polymer and graphene layers were weakly bound by van der Waals interactions, as summarized in Table 1. The adsorption energies of the polymer–graphene interfaces were analyzed by comparing the total energy of the interface system to the isolated system with a frozen interface structure. We defined the adsorption energy per carbon atom in the polymer backbone according to:

$$E_{\text{ads}} = -\frac{1}{N_{\text{C}}} (E_{\text{interface}} - E_{\text{graphene}}^{\text{i}} - E_{\text{polymer}}^{\text{i}}). \quad (1)$$

where, N_{C} is the number of carbon atoms that belonged to the polymer backbone inside the supercell, $E_{\text{interface}}$, $E_{\text{graphene}}^{\text{i}}$, and $E_{\text{polymer}}^{\text{i}}$ are the total energy of the polymer–graphene interface system, the energy of the isolated graphene structure, and the energy of the polymer structure, respectively.

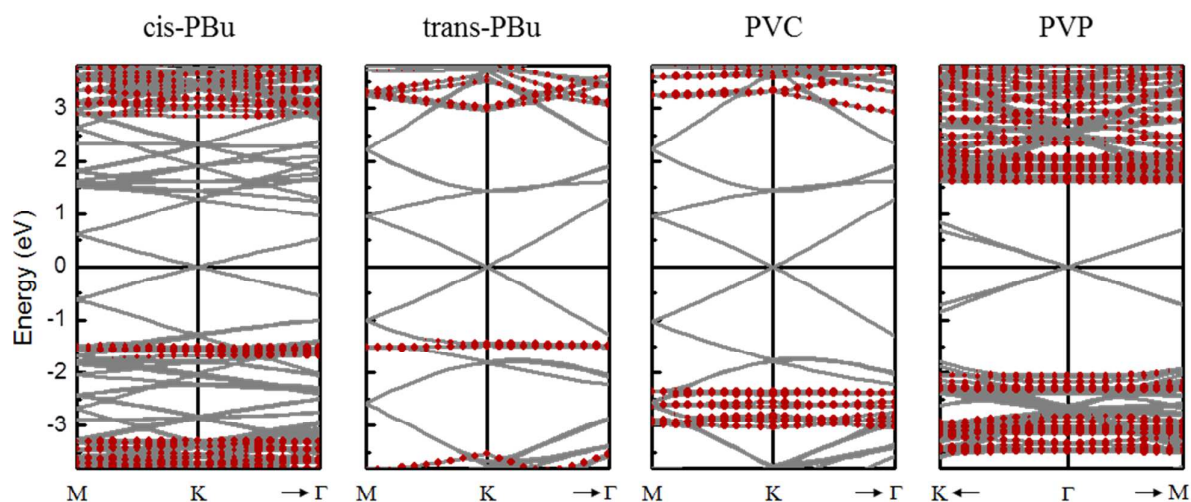


Figure S8. Band structure of the polymer-graphene system. Red dots indicate the major bands of the polymer.

I. Transfer of the free-standing CVD-grown graphene for the graphene-polymer system

(1) Preparing of Cu foil → (2) Spin-coating of the PMMA solution on the Cu foil → (3) Hole-pattern of the PMMA layer using the shadow mask and the O₂ plasma → (4) Etching of the Cu foil → (5) Transfer of the hole-patterned PMMA layer onto the graphene grown Cu foil → (6) Etching of the Cu foil → (7) Transfer of the free-standing graphene onto the substrate

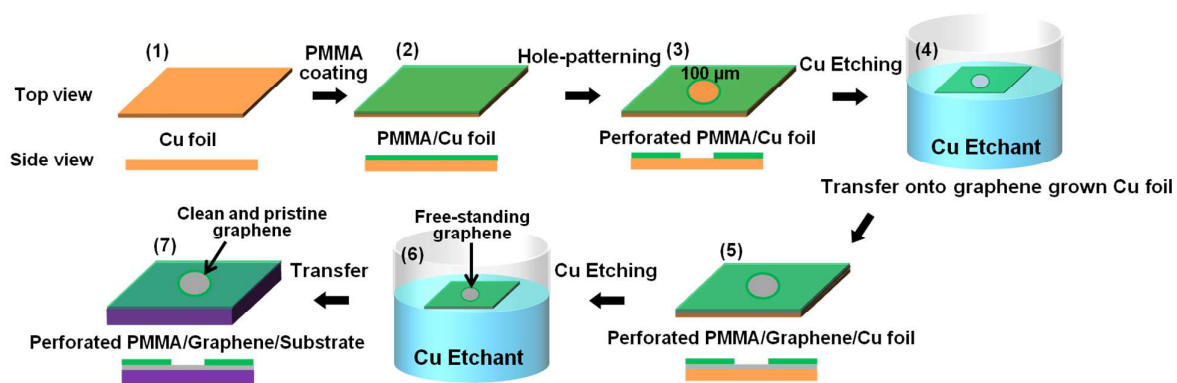


Figure S9. Scheme for transfer of the free-standing CVD-grown graphene

J. Graphene-polymer system *via* direct spin-coating of the polymer layers

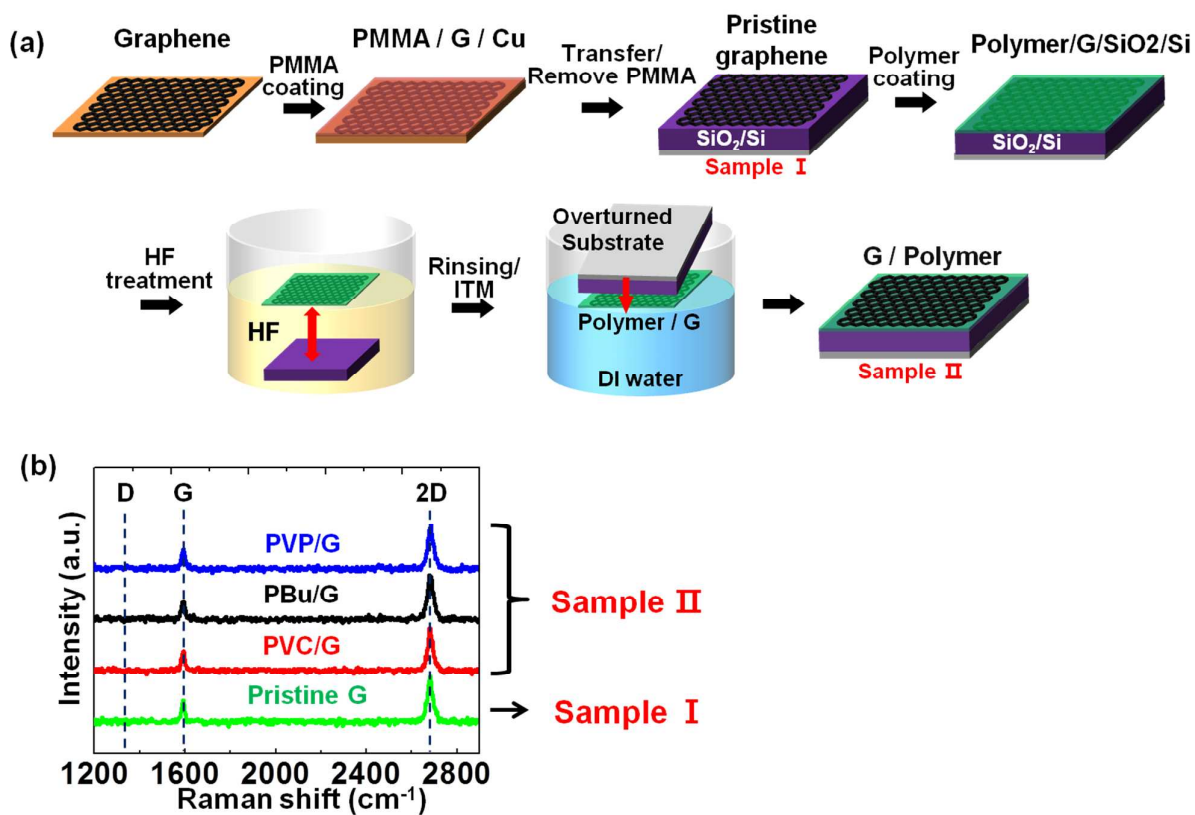


Figure S10. (a) Scheme for fabrication of graphene-polymer system. (b) Raman spectrum of pristine graphene (green), PVP (blue), PBU (black) or PVC (red) spin-coated graphene.

K. Band structure for polymer/graphene/Cu system

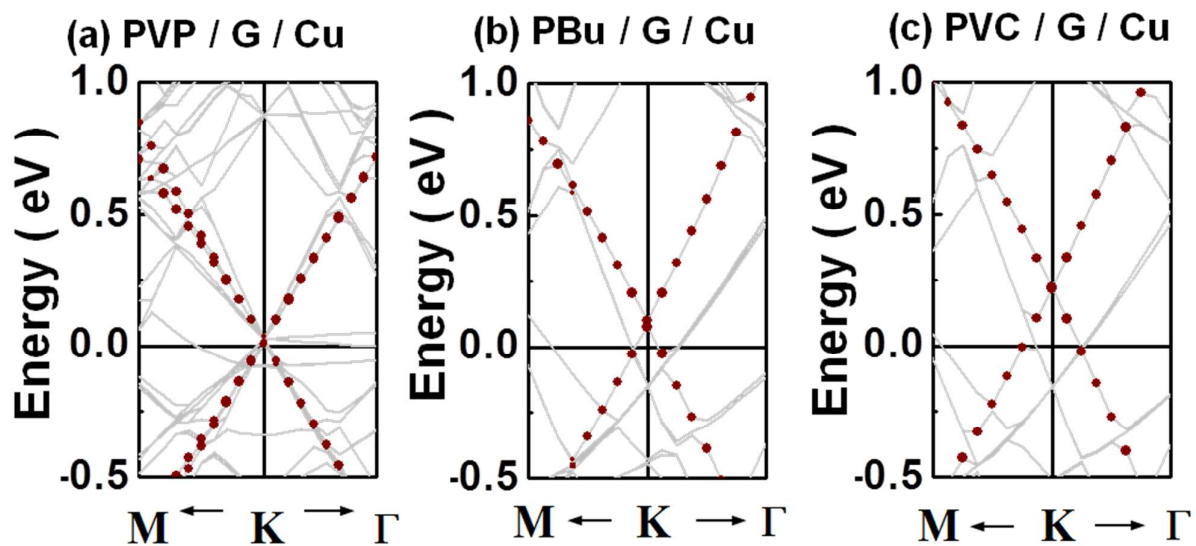


Figure S11. The Cu foil effects explain the observed graphene doping levels in the transport measurements. (a) PVP produced n-doping, and (c) PVC produced p-doping, relative to (b) PBU, which did not produce doping characteristics.

L. Fabrication of the pentacene FETs prepared with polymer-doped graphene electrodes.

The polymer/graphene film was transferred onto an HMDS-treated silicon substrate using the ITM. A defined sacrificial Al electrode pattern ($L = 100 \mu\text{m}$, $W = 1000 \mu\text{m}$) was deposited by thermal evaporation (30 nm). Subsequent O_2 plasma treatment removed the graphene, polymer, and HMDS layer except under the patterned Al area. Al was then etched away using CuCl_2 , and pentacene was deposited to form a semi-conducting channel (200 nm at 0.2 \AA/S).

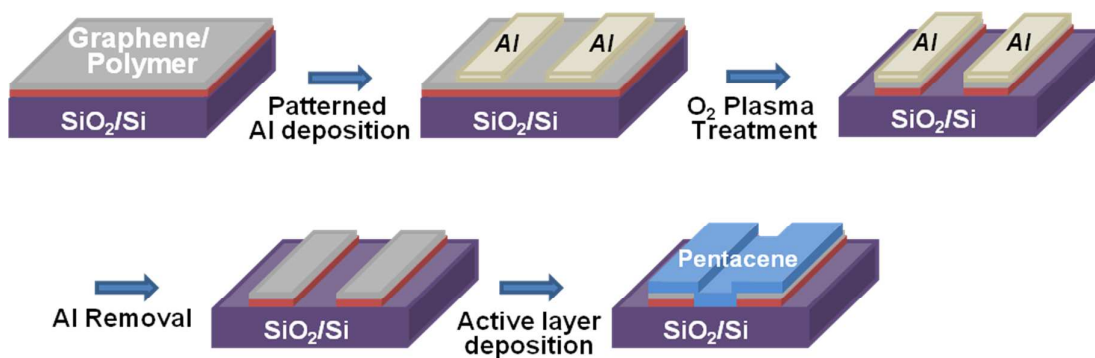


Figure S12. Schematic diagram of the process used to fabricate pentacene FETs from doped graphene electrodes prepared using the ITM.

M. Morphology of pentacene on graphene electrode and channel of bottom-contact pentacene FETs.

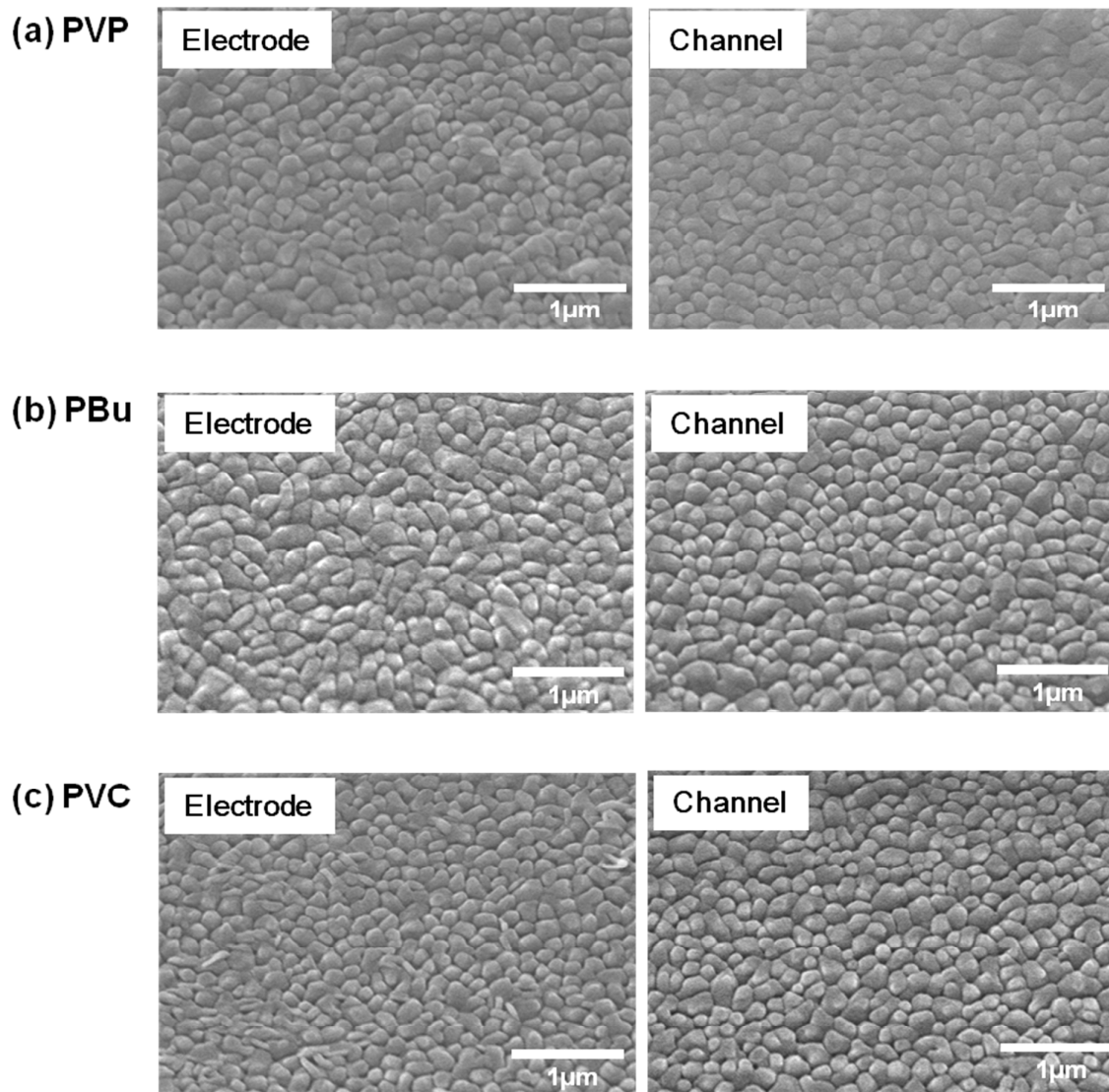


Figure S13. SEM images of pentacene on channel (HMDS) or graphene electrodes on PVP (a), PBU (b) or PVC (c).

N. Total resistance of pentacene FET with graphene electrode doped by different polymers

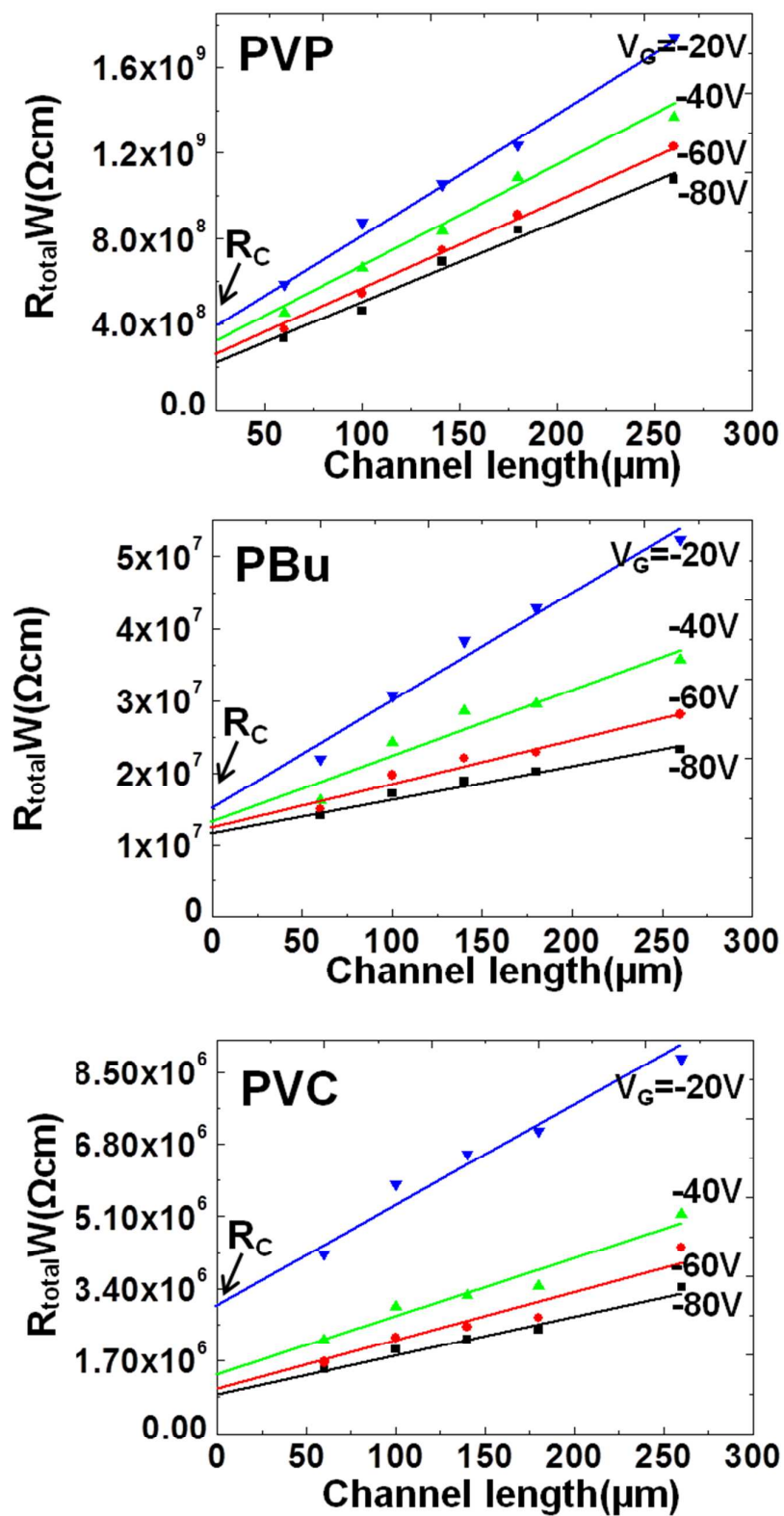


Figure S14. Channel width-normalized R_{total} obtained from the pentacene FETs prepared with graphene electrodes on (a) PVP, (b) PBu or (c) PVC.

REFERENCES

1. Kresse, G.; Furthmuller, J. Efficient Iterative Schemes for Ab-Initio Total-Energy Calculations using a Plane-Wave Basis Set. *Phys. Rev. B* **1996**, *54*, 11169-11186.
2. Dion, M.; Rydberg, H.; Schroder, E.; Langreth, D. C.; Lundqvist, B. I. Van der Waals Density Functional for General Geometries. *Phys. Rev. Lett.* **2004**, *92*, 246401-4.
3. Kresse, G.; Joubert, D. From Ultrasoft Pseudopotentials to the Projector Augmented-Wave Method. *Phys. Rev. B* **1999**, *59*, 1758-1775.
4. Klimes, J.; Bowler, D. R.; Michaelides, A. Van der Waals Density Functionals Applied to Solids. *Phys. Rev. B* **2011**, *83*, 195131-13.